PLOS ONE

Investigating the hard X-ray production via proton spallation on different materials to detect elements

Saeedeh Khezripour[1], Mohammadreza Rezaie[2], Mehdi Hassanpour[3]*,
Marzieh Hassanpour[3], Mohammad Rashed Iqbal Faruque[3]*, Mayeen Uddin Khandaker[4,5]*

1 Department of Molecular and Atomic Physics, Faculty of Modern Science and Technology, Graduate University of Advanced Technology, Kerman, Iran, 2 Department of Nuclear Engineering, Faculty of Modern Sciences and Technologies, Graduate University of Advanced Technology, Kerman, Iran, 3 Space Science Centre (ANGKASA), Institute of Climate Change (IPI), Universiti Kebangsaan Malaysia, Malaysia, Malaysia, 4 Centre for Applied Physics and Radiation Technologies, School of Engineering and Technology, Sunway University, Selangor, Malaysia, 5 Department of General Educational Development, Faculty of Science and Information Technology, Daffodil International University, Dhaka, Bangladesh

* mhassanpour67@yahoo.com (MH); rashed@ukm.edu.my (MRIF); mayeenk@sunway.edu.my (MUK)

Abstract

Various atomic and nuclear methods use hard (high-energy) X-rays to detect elements. The current study aims to investigate the hard X-ray production rate via high-energy proton beam irradiation of various materials. For which, appropriate conditions for producing X-rays were established. The MCNPX code, based on the Monte Carlo method, was used for simulation. Protons with energies up to 1650 MeV were irradiated on various materials such as carbon, lithium, lead, nickel, salt, and soil, where the resulting X-ray spectra were extracted. The production of X-rays in lead was observed to increase 16 times, with the gain reaching 0.18 as the proton energy increases from 100 MeV to 1650 MeV. Comparatively, salt is a good candidate among the lightweight elements to produce X-rays at a low proton energy of 30 MeV with a production gain of 0.03. Therefore, it is suggested to irradiate the NaCl target with 30 MeV proton to produce X-rays in the 0–2 MeV range.

Introduction

X-rays and their medical applications are significant in element detection [1, 2]. The X-ray scattering and diffraction (XRD) technique in crystallography can be used to analyse a crystal structure [3]. While the X-ray fluorescence (XRF) method, a non-destructive and fast technique, is widely used to determine the elemental composition of a material [4, 5]. Elements can be identified using proton or ion radiation on the target [6]. For instance, in the Proton Induced X-ray Emission (PIXE) and Proton Induced Gamma-ray Emission (PIGE) methods, the gamma and X-rays emitted from the activated materials at the nuclear and atomic levels were used for elemental analyses of the targets [7]. The generated gamma and X-rays or an ion beam are the primary tools for detecting elements. Generally, gamma and hard or soft X-rays are produced by irradiating high-energy electrons and protons on tungsten and other

materials [8–12]. The terms "hard X-ray" and "gamma ray" are commonly used to distinguish between sources of electromagnetic radiation. Specifically, X-rays are emitted due to the de-excitation of atomic electron levels around nuclei.

Contrarily, de-exciting nuclear levels of protons or neutrons in nuclides produces gamma rays. There are four possible ways for photon emission to occur when protons travel through a target material, namely: (a) through the de-excitation of atomic levels (i.e., X-ray emission); (b) through the de-excitation of nuclear levels (i.e., gamma-ray emission); (c) by the stopping of protons in the target (i.e., X-ray emission); and (d) through spallation processes, whereby secondary particles produced by the proton target interaction emit photons (i.e., both X-ray and gamma-ray emission). In the present study, all four mechanisms were observed following proton irradiation of the targets. Hence, it is impossible to differentiate between X-ray and gamma-ray emission in a mixed-field environment consisting of both types of radiation. Consequently, the emitted photons resulting from spallation processes were collectively referred to as "hard X-rays" or "gamma rays," with the former term being used in this study.

The energy of generated X-rays depends on the energy of the incident electron and proton beam. For instance, electron beams of up to 150 keV energy are used in industrial X-ray devices to produce X-rays in the same range [13]. Meanwhile, the electrons beam up to 15 MeV energy are used in the Varian accelerator to produce an X-ray in the same energy range [14]. Moreover, there are many reports on using radioactive elements as sources in element detection devices [15]. The radioactive elements are primarily used as the source due to eliminating high voltage and X-ray tubes to produce portable element detection devices. The proton source is the central part of elements detection in the PIXE method, where the intensity of the X-ray emitted from the target depends on the energy of the protons [16, 17]. Also, X-rays from the proton irradiation omitted on materials can be used as an X-ray source because the intensity depends on the energy and intensity of the irradiated protons. In a previous study, a neutron beam was employed to irradiate 162Er to produce a 163Ho isotope. The sample was irradiated to activate neutron for 104 s at the PSI spallation neutron source (SINQ) facility, following which the gamma spectra of the 162Er sample containing 163Ho isotope were recorded at various intervals of 5 h, 24 h, and 4 d post-irradiation [18]. The detection of elements was achieved through gamma spectra resulting from the spallation of a target under neutron irradiation. The neutron beam production was accomplished through proton beam irradiation of the spallation target [19]. In another study, Chiera et al. [20] measured the gamma rays produced by proton and neutron spallation of various targets for element detection purposes.

The present work analyses the hard X-ray spectrum emitted from the interaction of high-energy protons with several materials, such as soil, salt, and the elements available on the earth's surface, using the Monte Carlo method as a hard X-ray source. The hard X-ray source with proton collision can be introduced in two proton energy ranges: (a) hard X-ray source with the collision of the high-energy proton (up to 1 GeV) and (b) hard X-ray source with the collision of protons with energies less than 100 MeV. The collision of protons with different targets excites their nucleus, where the excited nucleus emits gamma rays with a specific energy spectrum [8]. Since proton absorption is possible by the target nucleus, the initial nucleus can be converted to a compound nucleus. The compound nucleus decays through various processes, including neutron emission, positive and negative beta particles, alpha particles, gamma emission, fission, etc. [21]. While increasing the proton energy may result in a spallation process for the compound nucleus [22, 23]. During the spallation process, the nucleus is converted into different elements. The spallation product is mainly at the excitation level and can be de-excited by emitting gamma and hard X-rays [24–29]. Usually, spallation has a specific threshold energy for every target [30]. The threshold energy of the spallation can be increased by increasing the element mass number. Recent studies calculated some elements'

photon production cross-section using the proton spallation process [16, 17]. The photon production rate due to the proton spallation process for many elements was also studied [31]. Hence, to choose the proper hard X-ray source in the present study based on the threshold energy for the proton spallation process of different targets, the hard X-ray energy spectrum emitted from many materials was studied using the Monte Carlo N-Particle Transport (MCNPX) code.

The MCNPX code is one of the most robust codes for nuclear calculations based on the Monte Carlo method. Several studies have used this code [32, 33] and reported experimental results versus simulations with greater accuracy [34]. This code is widely used in various fields like detectors [35], archaeology [36], food and dairy irradiation [37, 38], radiation shielding [39], and radiography and radiotherapy [40, 41]. The energy threshold and proper energy range to produce hard X-rays from proton spallation of NaCl, soil, and the well-known materials available in nature for the Photon Induced X-ray Florescence Emission (PIXFE) method [42–44] are described in this study.

Methods

A proton beam with surface energy distribution and different energies was irradiated on a cylinder with variable height and radius to produce X-rays. The proposed geometry was imported into the MCNPX code as an input file. The FT8 command was used in this code to activate the spallation process. This code together with the RES command [45] can trigger the production process of X-rays due to proton irradiation on various targets followed by the calculation of the produced particle spectrum. To determine the spallation products in the range of atomic numbers Z_1 to Z_2, the command RES Z_1 Z_2 was given after FT8. The general command was written as follows:

F8:h

FT8 RES Z_1 Z_2

where the h parameter is related to the proton spallation process, Tally F8 is a type of output command that indicates the pulse height or probability of the desired quantity, and FT8 is a command that activates the secondary particles produced by the irradiation of the primary particle on the target. If the command "RES Z_1 Z_2" is used, the secondary particles produced in the range of atomic numbers Z_1 to Z_2 will be displayed in the output. The results of proton spallation products were recorded in the output file as "ZAID S R (Atomic number×1000 +Math number)" by writing the above command in the input file of the MCNPX code and running it. The results reflect the characteristics of the atomic number and the mass number of spallation products, where "S" is the gain of products and "R" is the error of Monte Carlo calculations. When the number of particles for simulation was set to be 10^7, the resulting calculation error was recorded below 1%. It is possible to calculate the hard X-ray production with high accuracy due to the spallation process. After investigating the probability of the proton spallation process, the following command was used,

F2:P

e_2 E_{min} ni E_{max}

Where "p" indicates the produced photons, "e_2" is used to determine the spectrum of produced photons, and "ni" is the number of energy intervals. Whereas "E_{min}" is zero, "E_{max}" reflects the proton energy, and "ni" is the amount of each energy interval equivalent to 1 keV.

Due to the limited particles' energy level in the MCNPX code and to raise the energy of trackable particles, the PHYS command was used by defining a spherical surface around the target on which the proton was irradiated and the energy spectrum of X-ray was investigated using the *F2 command. Table 1 lists the data relating to the mass number, density, and

Table 1. The consistency between simulation and experimental results of photon production due to the spallation process of light nuclei [4, 8–12, 22, 23, 54, 55].

Spallation targets	Proton energy, Ep (MeV)	Produced photon energy (MeV)		
		Simulation	Experiment	Consistency (%)
^{28}Si	113	1.78	1.78	100
^{19}F	113	6.14	6.13	99
^{16}O	113	6.13	6.13	100
^{12}C	85	0.74	0.72	97%
		1	1.02	98%
		1.41	1.38	98%
		1.67	1.64	98%
		1.88	1.88	100%
		1.95	2.00	97%
		4.45	4.44	99%
		5.25	5.27	99%
^{7}Li	0.65–12	0.49	0.48	98%
	Median of consistency			98%

threshold energy of materials used in this research, including soil, salt, lead, lithium, etc. While Fig 1 depicts the geometry used in the present study. Cells 1 and 2 indicate calculating the X-ray spectrum produced in the target.

Cell 1 is characterised as a cylinder with a variable height and material with a radius of 20 cm. The proton source is situated as a surface source within this call with a 1 cm radius on the surface of the cylinder base. Since the rays stemming from the source are emitted perpendicularly to the cylinder base, the distribution of the source's surface is presumed to be uniform. Cell 2 which encircles the target, is classified as an air cell. Meanwhile, Cell 3 is a vacuum that envelops the outer space of the sphere measuring 40 cm in radius. In this cell, particle tracking is irrelevant and must not be considered in the simulation. The energy spectrum of the hard X-rays generated in the target reaching the surface of the cylinder's surrounding sphere can be ascertained using the command codes *F1 or *F2.

Results

Validation of a Monte Carlo program for hard X-ray production by spallation

The characteristic of hard X-ray spectrum obtained from the bombardment of ^{12}C by 85 MeV proton simulation result is reported and compared with the experimental results [46–48] as depicted in Table 1. The consistency between the present and experimental results was calculated for each hard X-ray peak, where the consistency was approximately 98%. Gamma-ray characteristics at 1.78 MeV energy were observed experimentally when ^{28}Si nuclei were bombarded with 113 MeV protons [49, 50]. The consistency between the simulation and experimental results was estimated at 100% (Table 1). The characteristics of gamma at 6.13 MeV energy each were experimentally measured by bombarding ^{19}F and ^{16}O nuclei with 113 MeV protons [51, 52]. The simulation results estimated the values of 6.13 MeV and 6.14 MeV for ^{16}O and ^{19}F, respectively. According to Table 1, the consistency was 100% and 99% for ^{16}O and ^{19}F, respectively. A characteristic gamma with an energy of 0.48 MeV was measured experimentally by bombarding ^{7}Li nuclei with protons in the range of 0.65 to 12 MeV energy [53]. The simulation results yielded an energy of 0.49 MeV for this range. Table 1 displays the overall consistency between the experimental and simulation results at 98%.
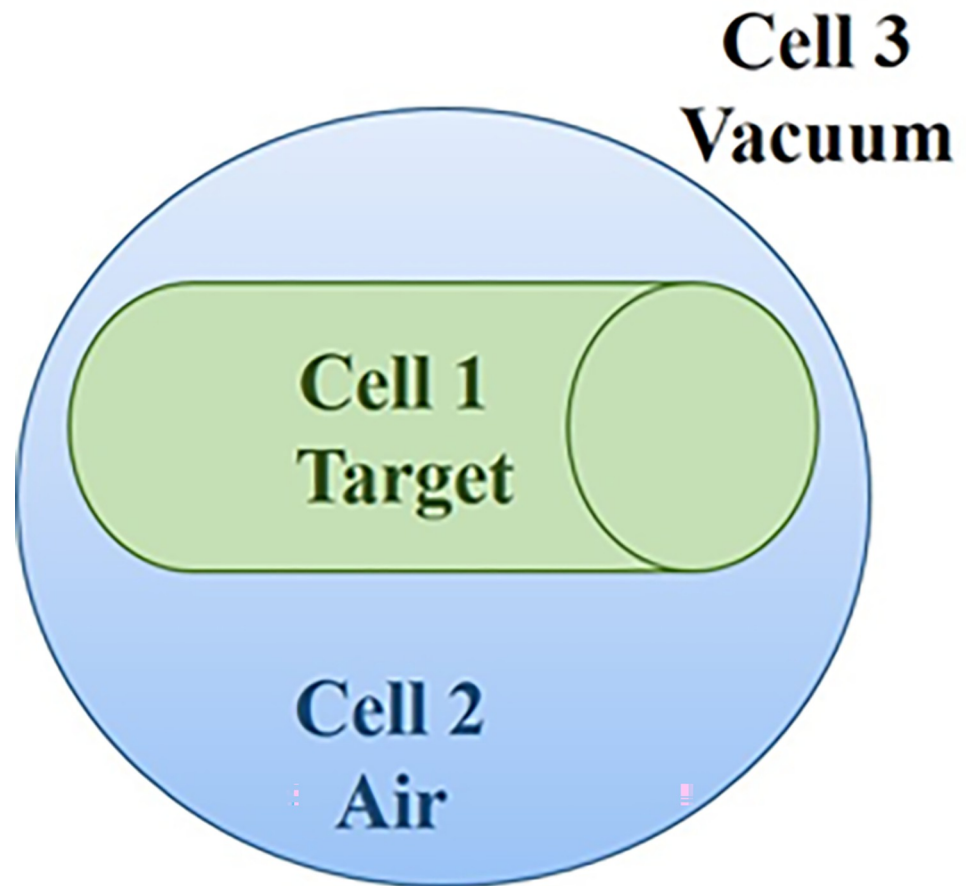
Fig 1. Representation of the cells defined in the MNCPX code for calculating X-ray spectrum.

According to Table 1, the average consistency between simulation and experimental results was 98%. Furthermore, the collision of carbon with a proton with 3–5 MeV energy can excite it to produce gamma-rays with an energy of 4.44 MeV [56], which is 100% consistent with the simulation results.

Hard X-ray production by proton beam spallation

The Monte Carlo method can be confidently used to check hard X-ray production with the bombardment of different nuclei by the proton beam due to its high percentage of consistency. Fig 2 illustrates the production of X-rays in the energy range of 0–4 MeV by irradiating a 600 MeV proton beam on a lead cylinder with a radius of 20 cm as a function of height (6, 12, 24, 50, 75, 100, 125, 150, and 180 cm). The X-ray production rate reached its optimal state by changing the height of the cylinder from 6 cm to 50 cm, producing three peaks at 0.54455, 0.87129, and 2.6139 MeV.

Fig 3 illustrates the X-ray production in the range of 0–4 MeV by a proton beam irradiated on a lead cylinder with a height of 50 cm as a function of energy ranging from 100 to 1650 MeV. The X-ray production increased by 16 times for the 1650 MeV proton beam compared to the 100 MeV proton.
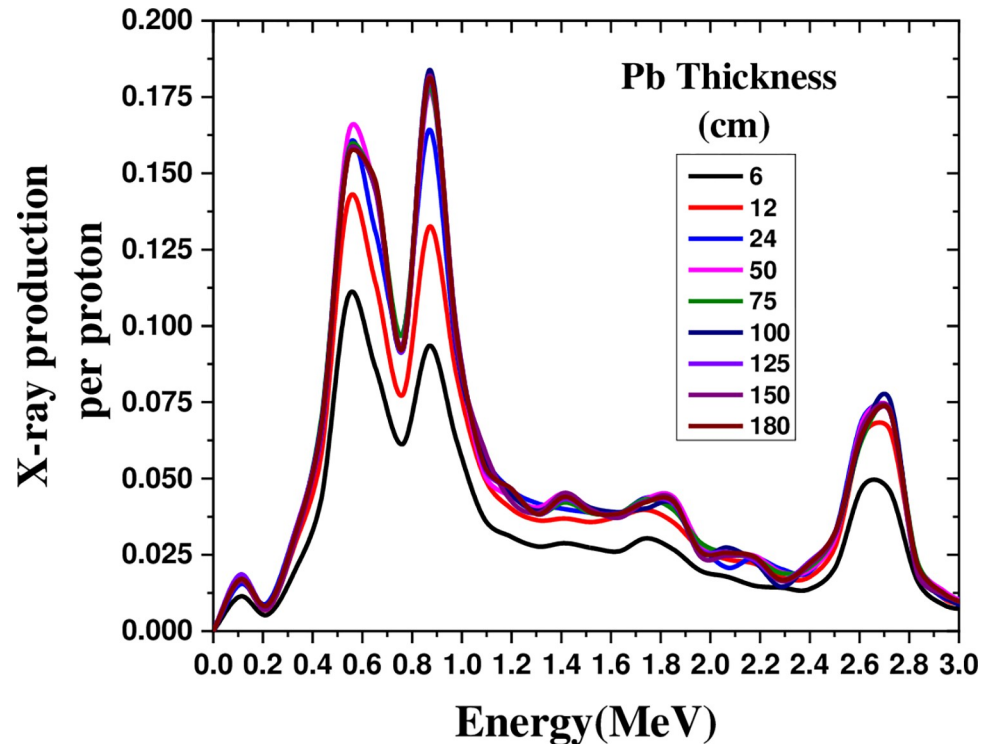
Fig 2. X-ray production in the energy range of 0–4 MeV by a 600 MeV proton beam irradiated on a lead cylinder with a radius of 20 cm and different cylinder heights.

Fig 4 depicts the X-ray production in the energy range of 0–6 MeV by irradiating a 600 MeV proton beam on lead and carbon, which produced X-rays in the lead, 16 times higher than in carbon.

Fig 5 represents the X-ray production in the 0–8 MeV range by a 40 MeV proton beam on salt and lithium. The salt spectrum, which peaked at 0.22 MeV, was observed to be higher than the lithium peak at 0.5 MeV.

Fig 6 represents the X-ray production in the energy range of 0–5 MeV by a 600 MeV proton beam on nickel. Nickel's spectrum peaked at 0.33 MeV, with a proper X-ray production in the 0–2 MeV range.

Fig 7 depicts the X-ray production in the energy range of 0–5 MeV by irradiating 30 MeV and 317 MeV proton beams on salt. By increasing the proton energy by 10.57 times, the salt spectrum peaked at 0.22 MeV, nearly crossed by six times.

Fig 8 depicts the X-ray production in the energy range of 0–5 MeV by irradiating a 100 MeV proton beam on salt and lead. It revealed that the salt spectrum peak at 0.3 MeV was six times higher than in lead.

Fig 9 displays the X-ray production in the 0–5 MeV range by irradiating 50 MeV and 200 MeV proton beams on the soil. The increment of energy by four times spiked the spectrum peak at 0.30 MeV by nearly 18 times.

Fig 10 depicts the X-ray production in the range of 0–5 MeV by a proton beam on salt, lithium, and soil at the threshold energy for spallation (Table 1). The spectrum peak for salt was six times than that of lithium. Besides that, salt yielded maximum X-ray production gain due to spallation at the threshold energy (Table 2).
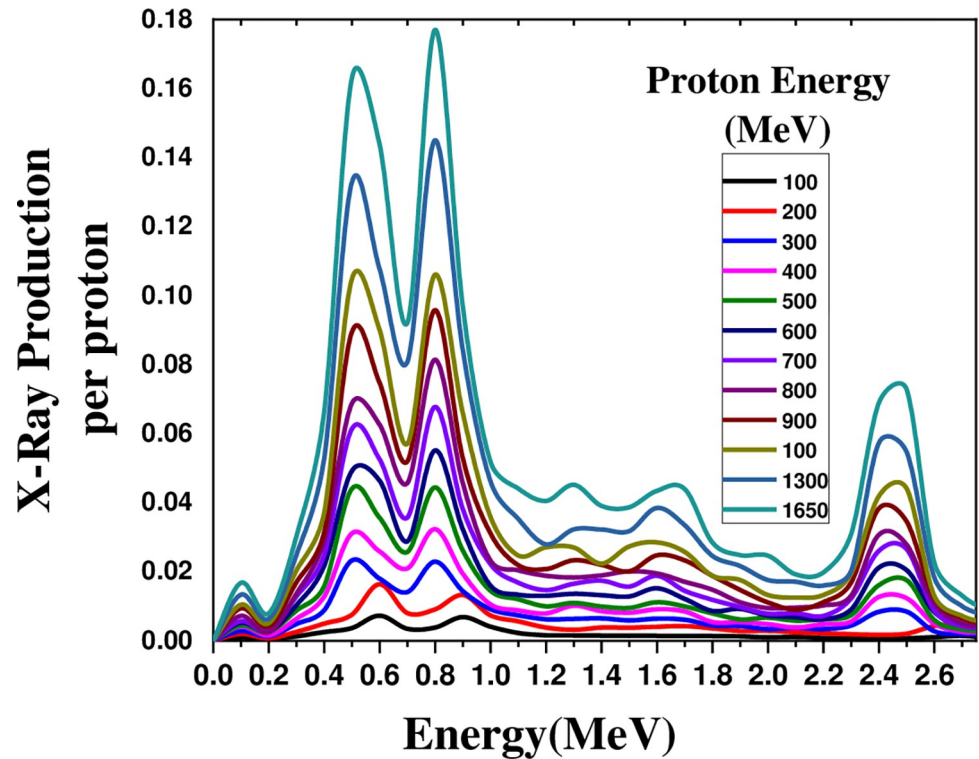
Fig 3. The X-ray production in the energy range of 0–4 MeV by a proton beam energy ranging from 100 to 1650 MeV, irradiated on a 50 cm lead cylinder.

Discussion

Table 2 lists the results obtained for X-ray production by the spallation process using light and heavy materials.

The heavy elements yield higher X-ray production than light elements as the proton energy is increased. Contrarily, the light elements have less X-ray production gain than heavy elements with decreased proton energy. In the proton energy range of 159–294 MeV, the X-ray production gain through spallation in salt was almost equal to that of lead with a proton energy of 1650 MeV. Based on the X-rays produced through proton spallation, it is recommended to use salt, soil, lead, and nickel. The results indicated that salt and lead with maximum X-ray production gain at 0.22 MeV (0–0.4 MeV range) and 0.87 MeV (0–2.5 MeV range) are good candidates for detecting elements via the PIXFE method.

Conclusion

X-ray has many applications in science and technology. There are different ways to produce X-rays. One of the methods is to stop charged particles in other targets. When charged particles collide with atoms and nuclei, they are excited and emit X-rays and gamma-rays. To date, limited studies have investigated the effect of spallation on X-ray production. This study investigated the possibility of producing hard X-rays by activating the proton spallation process with different energies. During the spallation process, the target nuclei were evaporated by absorbing the energy of incident particles such as protons. In the process of nuclear evaporation, hard X-rays were also emitted in addition to producing nuclei with a mass number lower than the target mass number. For this purpose, the hard X-ray production was investigated
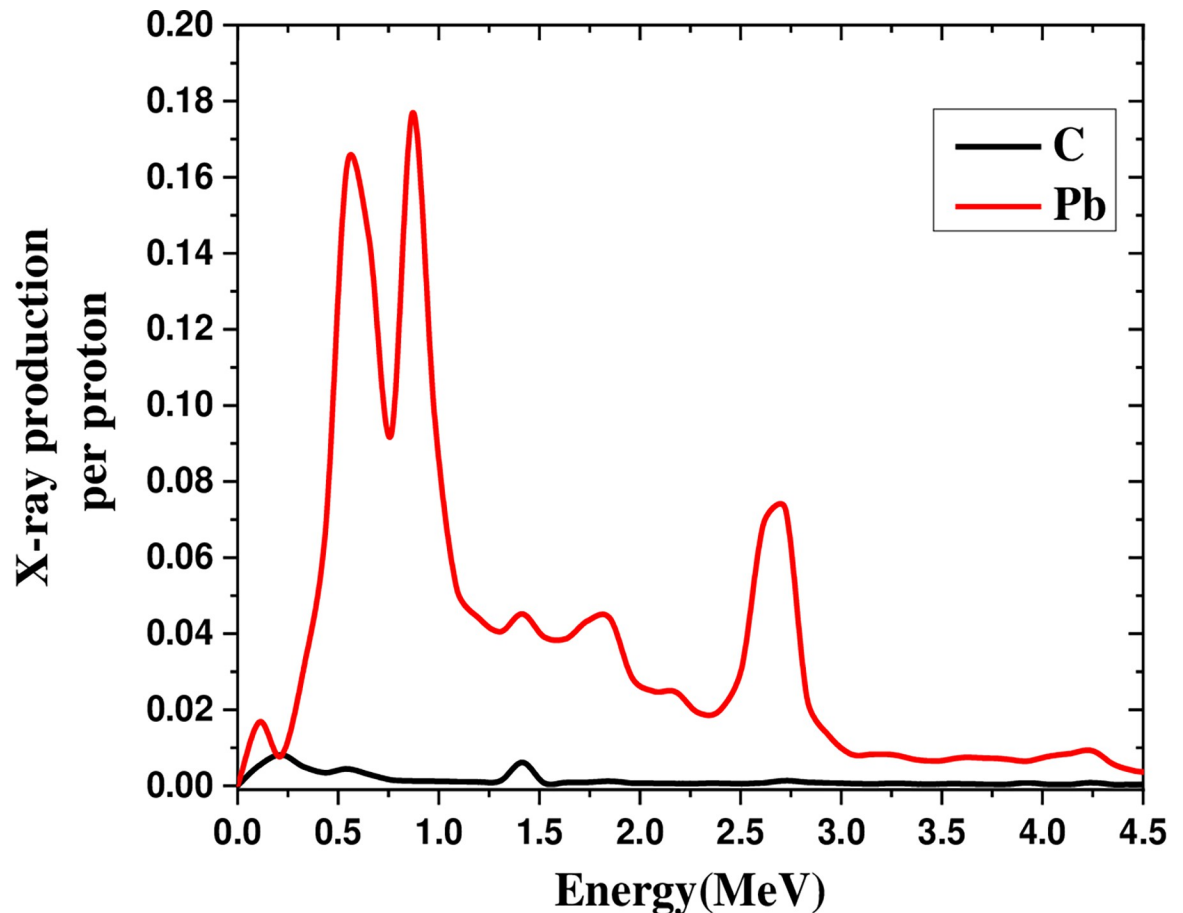
Fig 4. Comparison of X-ray production in the 0–6 MeV range by irradiating 600 MeV proton beam on lead and carbon.

https://doi.org/10.1371/journal.pone.0288287.g004

due to proton beam irradiation on heavy, light, and mixed targets without considering the produced nuclei. Lead and nickel were the heavy, and lithium and carbon were the light nuclei used in this study. The combination of light nuclei that was used was NaCl. Furthermore, soil was chosen as the combination of heavy and light nuclei. The spallation process in heavy nuclei is possible when the energy of incident protons are higher than the proton energy of light nuclei, depending on the binding energy of nuclei. Consequently, the heavy lead and nickel nuclei have been irradiated by protons in the range of energy 100–1600 MeV, and 600 MeV, respectively, to produce a hard X-ray.

On the other hand, light carbon and lithium nuclei were irradiated with 600 and 40 MeV proton beams to produce hard X-rays. Also salt and soil were irradiated by a proton beam in the energy range of 30–317 MeV and 50–200 MeV, respectively, to produce hard X-rays. Based on the results, the hard X-ray spectrums were in the energy range of 0–8 MeV, where their peaks depended on the material and proton beam energy. The hard X-ray spectrum produced by the heavy elements with high-energy protons was similar to the hard X-ray spectrum produced by the light elements with low-energy protons. Hence, it was concluded that salt and lead yielded the maximum hard X-ray production gain due to the proton spallation. Salt was the best candidate for hard X-ray production due to the lower energy proton beam and higher hard X-ray production gain than the other materials. For 317 MeV proton irradiation on salt, the most probability interval energy of produced hard X-ray is 0–0.4 MeV. The hard X-ray
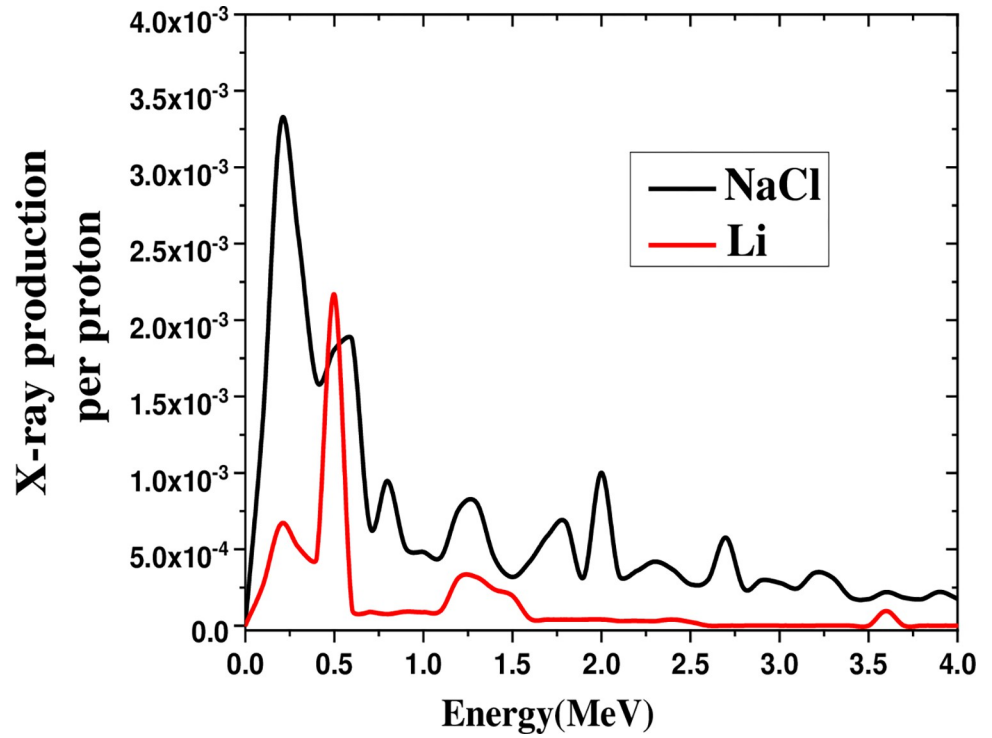
Fig 5. Comparison of X-ray production in the 0–8 MeV range by irradiating 40 MeV proton beam on salt and lithium.
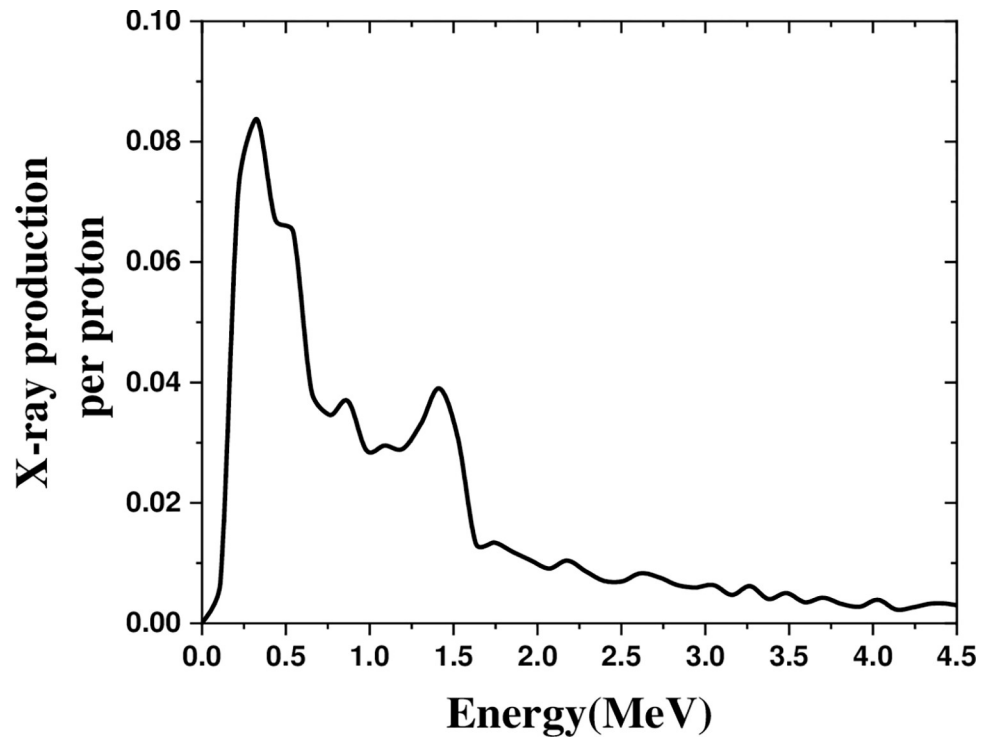
Fig 6. The X-ray production in the range of 0–5 MeV by irradiating 600 MeV proton beam on nickel.
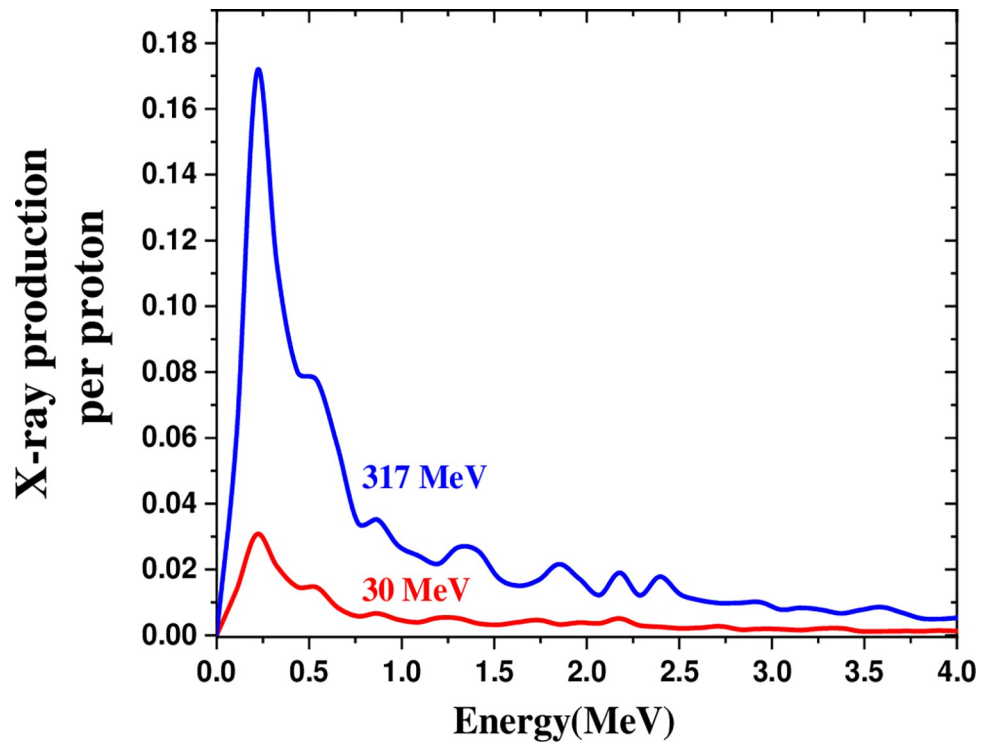
Fig 7. The X-ray production in the energy range of 0–5 MeV by irradiating 30 MeV and 317 MeV proton beams on salt.

https://doi.org/10.1371/journal.pone.0288287.g007
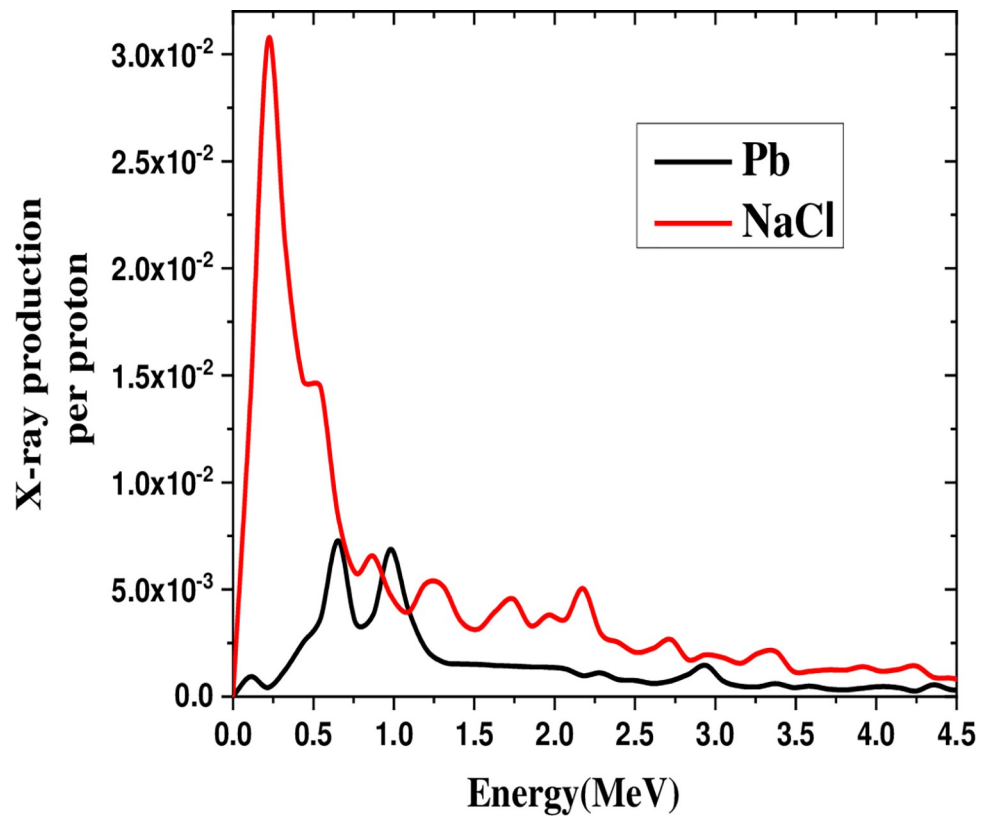
Fig 8. Comparison of X-ray production in the 0–5 MeV range by irradiating 100 MeV proton beam on salt and lead.

https://doi.org/10.1371/journal.pone.0288287.g008

Fig 9. X-ray production in the energy range of 0–5 MeV by the 50 and 200 MeV proton beams on soil.

Fig 10. The X-ray production in the energy range of 0–5 MeV by the proton beam on soil, lithium, and salt in the energy threshold for spallation.
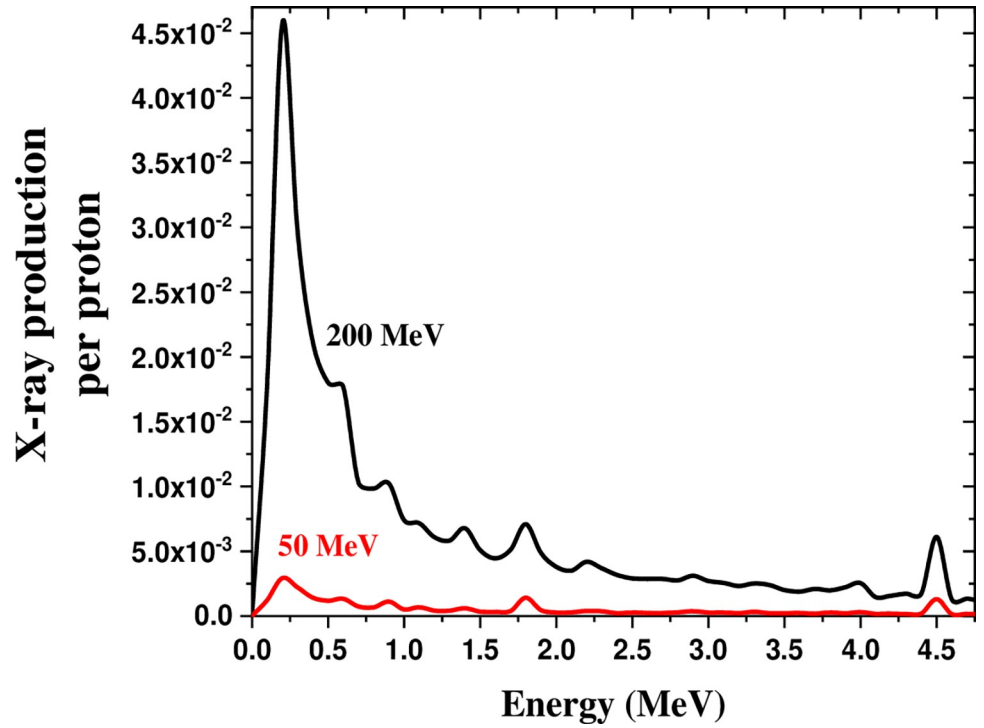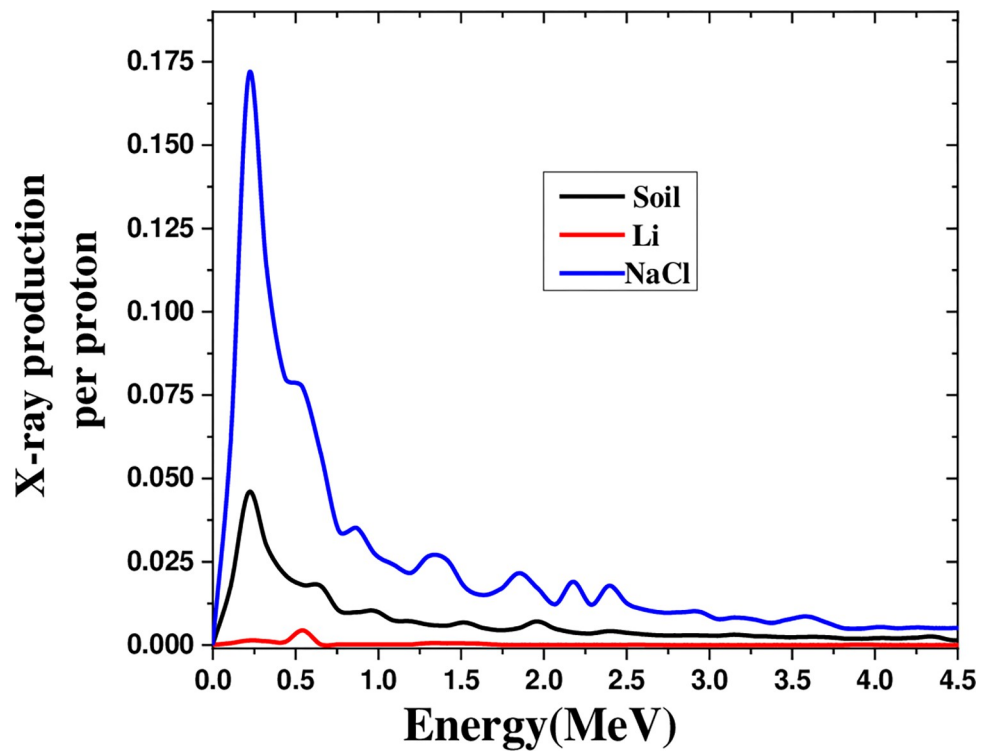
Table 2. X-ray production through the spallation process using different materials.

Material	Mass Number	Density (g/cm³)	Threshold energy of spallation (MeV) [22, 23]	Proton beam energy (MeV)	X-ray production Gain at the peak energy	peak energy (MeV)	Most probability interval energy of produced X-ray (MeV)
Lead	207	11.34 [57]	1630	100–1650	0.18	0.87	0–2.5
Nickel	58	8.90 [58]	506	600	0.084	0.33	0–2.5
Lithium	7	0.53 [59]	39	40	0.00134	0.50	0–0.6
Carbon	12	2.30 [60]	90	600	0.008	0.22	0–1.85
Salt	-	2.17 [61]	159–294	30–317	0.17	0.22	0–0.4
Soil	-	2.26 [62]	90–491	50–200	0.046	0.30	0–2.94

https://doi.org/10.1371/journal.pone.0288287.t002

production gain at peak energy (0.22 MeV) was 0.17. Therefore, 0–0.4 MeV energy for hard X-ray by proton irradiation on salt is a good candidate for detecting elements by the PIXFE method.

Supporting information

S1 File.
(ZIP)

Author Contributions

Conceptualization: Saeedeh Khezripour, Mohammadreza Rezaie, Mehdi Hassanpour, Marzieh Hassanpour.

Data curation: Saeedeh Khezripour, Mohammadreza Rezaie, Mehdi Hassanpour, Marzieh Hassanpour.

Formal analysis: Saeedeh Khezripour, Mohammadreza Rezaie, Mehdi Hassanpour, Marzieh Hassanpour.

Funding acquisition: Mohammad Rashed Iqbal Faruque.

Investigation: Saeedeh Khezripour, Mohammadreza Rezaie, Mehdi Hassanpour, Marzieh Hassanpour.

Methodology: Saeedeh Khezripour, Mohammadreza Rezaie, Mehdi Hassanpour, Marzieh Hassanpour, Mohammad Rashed Iqbal Faruque, Mayeen Uddin Khandaker.

Project administration: Saeedeh Khezripour, Mohammadreza Rezaie, Mehdi Hassanpour, Mohammad Rashed Iqbal Faruque, Mayeen Uddin Khandaker.

Resources: Saeedeh Khezripour, Mohammadreza Rezaie, Mehdi Hassanpour, Marzieh Hassanpour, Mohammad Rashed Iqbal Faruque, Mayeen Uddin Khandaker.

Software: Saeedeh Khezripour, Mohammadreza Rezaie, Mehdi Hassanpour, Marzieh Hassanpour.

Supervision: Mohammadreza Rezaie, Mohammad Rashed Iqbal Faruque, Mayeen Uddin Khandaker.

Validation: Saeedeh Khezripour, Mohammadreza Rezaie, Mehdi Hassanpour, Marzieh Hassanpour, Mohammad Rashed Iqbal Faruque, Mayeen Uddin Khandaker.

Visualization: Mohammadreza Rezaie, Mehdi Hassanpour, Marzieh Hassanpour, Mohammad Rashed Iqbal Faruque, Mayeen Uddin Khandaker.

Writing – original draft: Saeedeh Khezripour, Mehdi Hassanpour, Marzieh Hassanpour.

Writing – review & editing: Mohammadreza Rezaie, Mohammad Rashed Iqbal Faruque, Mayeen Uddin Khandaker.

References

1. Procz S., Avila C., Fey J., Roque G., Schuetz M. and Hamann E., (2019). X-ray and gamma imaging with Medipix and Timepix detectors in medical research. Radiation Measurements, 127, p.106104.

2. Laird J.S., Hughes A.E., Ryan C.G., Visser P., Terryn H. and Mol J.M.C., (2017). Particle induced gamma and X-ray emission spectroscopies of lithium based alloy coatings. Nuclear Instruments and Methods in Physics Research Section B: Beam Interactions with Materials and Atoms, 404, pp.167–172.

3. Iwashita N. X-ray powder diffraction. In Materials science and engineering of carbon. Butterworth-Heinemann. (2016) pp. 7–25.

4. Fernández-Ruiz R. Quantitation of the production cross-section and transition probabilities of the L and M X-ray series in the Au (0) and Au (3+) atomic environments using Total-reflection X-ray fluorescence. Spectrochimica Acta Part B: Atomic Spectroscopy. 180 (2021) p.106207.

5. Kelly S.D., Hesterberg D. and Ravel B. Analysis of soils and minerals using X-ray absorption spectroscopy. Methods of soil analysis part 5—mineralogical methods. 5 (2008) pp.387–463.

6. Magalhaes Martins P., Dal Bello R., Ackermann B., Brons S., Hermann G., Kihm T. et al. PIBS: Proton and ion beam spectroscopy for in vivo measurements of oxygen, carbon, and calcium concentrations in the human body. Scientific reports. 10(1) (2020) pp.1–14.

7. Walter P., Variola A., Zomer F., Jaquet M. and Loulergue A. A new high quality X-ray source for cultural heritage. Comptes Rendus Physique. 10(7) (2009) pp.676–690.

8. Koehler K.E., Yoho M.D., Carpenter M.H., Croce M.P., Mercer D.J., Smith C.M., et al. New Experimentally Observable Gamma-ray Emissions from 241Am Nuclear Decay. (2021). arXiv preprint arXiv:2103.15893.

9. Miranda J., De Lucio O.G. and Lugo-Licona M.F. X-ray production induced by heavy ion impact: challenges and possible uses. Revista mexicana de física. 53 (2007) pp.29–32.

10. Grigoriadis A., Andrianaki G., Tatarakis M., Benis E.P. and Papadogiannis N.A. Betatron-type laser-plasma x-ray sources generated in multi-electron gas targets. Applied Physics Letters. 118(13) (2021) p.131110.

11. International Agency for Research on Cancer. A Review of Human Carcinogens. F. Chemical Agents and Related Occupations: IARC Monographs on the Evaluation of Carcinogenic Risks to Humans. (2012).

12. Pellegrini C. On some methods of x-ray production from relativistic electron beams. Journal of X-Ray Science and Technology. 4(4) (1994) pp.275–289. https://doi.org/10.3233/XST-1994-4403 PMID: 21307465

13. Kantsyrev V. L., Fedin D. A., Shlyaptseva A. S., Hansen S., Chamberlain D., and Ouart N. "Energetic electron beam generation and anisotropy of hard x-ray emission from 0.9 to 1.0 MA high-ZX pinches." *Physics of Plasmas* 10, no. 6 (2003): 2519–2526.

14. Sihaloho K. May. Evaluation of photon and neutron dose distribution from the Varian Clinac 2300EX 15 MV medical LINAC with MCNP6 Code. In Journal of Physics: Conference Series (2021) (Vol. 1912, No. 1, p. 012011). IOP Publishing.

15. Dehghan H.R., Negarestani A. and Rezaie M.R. Study of the possibility of using IXRF technique to detect the elements present in dust using Monte Carlo N Particles. BULGARIAN CHEMICAL COMMUNICATIONS. 49(4) (2017) pp.874–878.

16. Heil M., Reifarth R., Fowler M.M., Haight R.C., Käppeler F., Rundberg R.S., et al. A 4πBaF2 detector for (n, γ) cross-section measurements at a spallation neutron source. Nuclear Instruments and Methods in Physics Research Section A: Accelerators, Spectrometers, Detectors and Associated Equipment. 459(1–2) (2001) pp.229–246.

17. Miceli A., Festa G., Senesi R., Cippo E.P., Giacomelli L., Tardocchi M., et al. Measurements of gamma-ray background spectra at spallation neutron source beamlines. Journal of Analytical Atomic Spectrometry. 29(10) (2014) pp.1897–1903.

18. Heinitz S., Kivel N., Schumann D., Köster U., Balata M., Biasotti M., et al., 2018. Production and separation of 163Ho for nuclear physics experiments. *PLoS one*, 13(8), p.e0200910. https://doi.org/10.1371/journal.pone.0200910 PMID: 30133443

19. Li X., Wan J., Zhang S., Lin P., Zhang Y., Yang G., et al., 2017. Preliminary research on flow rate and free surface of the accelerator driven subcritical system gravity-driven dense granular-flow target. *Plos one*, 12(11), p.e0187435. https://doi.org/10.1371/journal.pone.0187435 PMID: 29095910

20. Chiera N.M., Talip Z., Fankhauser A. and Schumann D., 2020. Separation and recovery of exotic radiolanthanides from irradiated tantalum targets for half-life measurements. *Plos one*, 15(7), p.e0235711. https://doi.org/10.1371/journal.pone.0235711 PMID: 32645091

21. Moro R., Brondi A., Gelli N., Barbui M., Boiano A., Cinausero M., et al. Compound nucleus evaporative decay as a probe for the isospin dependence of the level density. The European Physical Journal A. 48 (11) (2012) pp.1–8.

22. Kondev F.G. and Naimi S. The AME2016 atomic mass evaluation (II). Tables, graphs and references. Chinese Physics C. 41(3) (2017) p.030003.

23. Mongelli S.T., Maiorino J.R., Anéfalos S., Deppman A. and Carluccio T. Spallation physics and the ADS target design. Brazilian Journal of Physics. 35 (2005) pp.894–897.

24. Filges D., Goldenbaum F., Enke M., Galin J., Herbach C.M., Hilscher D., et al. Spallation neutron production and the current intra-nuclear cascade and transport codes. The European Physical Journal A-Hadrons and Nuclei. 11(4) (2001) pp.467–490.

25. Apostalakis J., Ivantchenko A., Ivanchenko V.N., Kossov M., Quesada J.M. and Wright D.H. May. Geant4 simulation of nuclear spallation reactions. In Proc. International Topical Meeting on Nuclear Research Applications and Utilization of Accelerators. Satellite Meeting on Spallation Reactions. (2009) pp. 4–8.

26. Benlliure J. Spallation reactions in applied and fundamental research. In The Euroschool Lectures on Physics with Exotic Beams, Vol. II (2006) pp. 191–238. Springer, Berlin, Heidelberg.

27. Gloris M., Michel R., Sudbrock F., Herpers U., Malmborg P. and Holmqvist B. Proton-induced production of residual radionuclides in lead at intermediate energies. Nuclear Instruments and Methods in Physics Research Section A: Accelerators, Spectrometers, Detectors and Associated Equipment. 463 (3) (2001) pp.593–633.

28. Ogawa T., Hashimoto S., Sato T. and Niita K. Development of gamma de-excitation model for prediction of prompt gamma-rays and isomer production based on energy-dependent level structure treatment. Nuclear Instruments and Methods in Physics Research Section B: Beam Interactions with Materials and Atoms. 325 (2014) pp.35–42.

29. Karamian S.A. and Ur C.A. Production of isomers by spallation and consequences for nuclear science and applications. International Journal of Theoretical Physics, Group Theory, and Nonlinear Optics. 16 (1/2) (2012) p.1.

30. Ophoven N., Mauerhofer E., Li J., Rücker U., Zakalek P., Baggemann J., et al. Monte Carlo simulation of proton-and neutron-induced radiation damage in a tantalum target irradiated by 70 MeV protons. Applied Physics A. 127(8) (2021) pp.1–14.

31. Muçogllava B. A novel layered boron-based neutron shield design and results from neutron and gamma irradiation studies (Master's thesis, Middle East Technical University). (2022).

32. Khezripour S., Negarestani A. and Rezaie M.R. Investigating the response of Micromegas detector to low-energy neutrons using Monte Carlo simulation. Journal of Instrumentation. 12(08) (2017) p. P08007.

33. Khezripour S., Zarei N., and Rezaie M.R. "Estimation of granite radiation hazards of Deh Siahan village in Rafsanjan city." Journal of Instrumentation 17. 08 (2022) T08011.

34. Hassanpour M., Hassanpour M., Rezaie M., Salajegheh E., Faruque M.R.I., Khandaker M.U. et al. Studies of the mechanical and neutron shielding features of concrete by incorporation of green additive materials: Experimental and numerical study. Radiation Physics and Chemistry. 191 (2022) p.109846.

35. Hassanpour M., Dehghanipour P., Rezaie M., Hassanpour M., Faruque M.R.I. and Khandaker M.U. Study of alpha spectrometry for detection of radon and progeny using gas micro-strip detector. Applied Radiation and Isotopes. (2022) p.110344. https://doi.org/10.1016/j.apradiso.2022.110344 PMID: 35764003

36. Hassanpour M., Khezripour S., Rezaie M., Hassanpour M., Faruque M.R.I. and Khandaker M.U. The efficacy of thick gas electron multiplier detector in measuring 14C for dating purpose. Radiation Physics and Chemistry. (2022) p.110288.

37. Hassanpour M., Rezaie M., Faruque M.R.I. and Khandaker M.U. A novel approach for the reduction of aflatoxin in pistachio nuts using experimental and MCNP simulation. Radiation Physics and Chemistry. 189 (2021) p.109752.

38. Hassanpour M., Rezaie M.R. and Baghizadeh A. Practical analysis of aflatoxin M1 reduction in pasteurized Milk using low dose gamma irradiation. Journal of Environmental Health Science and Engineering. 17(2) (2019) pp.863–872. https://doi.org/10.1007/s40201-019-00403-9 PMID: 32030159

39. Hassanpour Ma., Hassanpour Me., Faghihi S., Khezripour S., Rezaie M.R., Dehghanipour P., et al. "Introduction of Graphene/h-BN Metamaterial as Neutron Radiation Shielding by Implementing Monte Carlo Simulation." Materials 15, no. 19 (2022) 6667. https://doi.org/10.3390/ma15196667 PMID: 36234009

40. Azadegan N., Hassanpour M., Khandaker M.U., Faruque M.R.I., Al-mugren K.S. and Bradley D.A. Calculation of secondary radiation absorbed doses due to the proton therapy on breast cancer using MCNPX code. Radiation Physics and Chemistry. 183 (2021) p.109427.

41. Khandaker M.U., Hassanpour Me., Khezripour S., Rezaei M.R.,Bazghandi A., Hassanpour Ma., et al. "Investigation of the effect of 131I on blood parameters for thyroid cancer treatment." Radiation Physics and Chemistry. (2023) 110897.

42. Marchais T, Pérot B, Carasco C, Ma JL, Allinei PG, Toubon H, et al. The use of self-induced X-ray fluorescence in gamma-ray spectroscopy of uranium ore samples. InEPJ Web of Conferences 2020 (Vol. 225, p. 05003). EDP Sciences.

43. Hans Andreas, Schmidt Philipp, Ozga Christian, Hartmann Gregor, Holzapfel Xaver, Ehresmann Arno, et al. "Extreme ultraviolet to visible dispersed single photon detection for highly sensitive sensing of fundamental processes in diverse samples." Materials 11, no. 6 (2018): 869.

44. Sun Yu-Ping, Rinkevicius Zilvinas, Wang Chuan-Kui, Carniato Stephane, Simon Marc, Taieb Richard, et al. "Two-photon-induced x-ray emission in neon atoms." Physical Review A 82, no. 4 (2010): 043430.

45. Pelowitz D.B., 2005. MCNPXTM user's manual. Los Alamos National Laboratory, Los Alamos, 5, p.369.

46. Verburg J.M., Shih H.A. and Seco J. Simulation of prompt gamma-ray emission during proton radiotherapy. Physics in Medicine & Biology. 57(17) (2012) p.5459. https://doi.org/10.1088/0031-9155/57/17/5459 PMID: 22864267

47. Belhout A., Kiener J., Coc A., Duprat J., Engrand C., Fitoussi C., et al. γ-ray production by proton and α-particle induced reactions on C 12, O 16, Mg 24, and Fe. Physical Review C, 76(3) (2007) p.034607.

48. Aharonian F.A. and Sunyaev R.A. Gamma-ray line emission, nuclear destruction and neutron production in hot astrophysical plasmas. The deuterium boiler as a gamma-ray source. Monthly Notices of the Royal Astronomical Society, 210(2) (1984) pp.257–277.

49. Freitas H.F.M. Prompt Gamma-Ray Spectroscopy in Proton Therapy for Prostate Cancer. (2020).

50. Penninckx S., Hespeels F., Smeets J., Colaux J.L., Lucas S. and Heuskin A.C. Metallic Nanoparticles: A Useful Prompt Gamma Emitter for Range Monitoring in Proton Therapy? Radiation. 1(4) (2021) pp.305–316.

51. Pham M. Gamma ray production cross sections of proton bombardment of fluorine for light element analysis and depth profiling (Doctoral dissertation, Massachusetts Institute of Technology). (2019).

52. Polf J.C., Panthi R., Mackin D.S., McCleskey M., Saastamoinen A., Roeder B.T., et al. Measurement of characteristic prompt gamma rays emitted from oxygen and carbon in tissue-equivalent samples during proton beam irradiation. Physics in Medicine & Biology. 58(17) (2013) p.5821. https://doi.org/10.1088/0031-9155/58/17/5821 PMID: 23920051

53. Chadwick G.B., Alexander T.K. and Warren J.B. Gamma radiation from the proton bombardment of boron ten. Canadian Journal of Physics. 34(4) (1956) pp.381–388.

54. Ricciardi M.V., Armbruster P., Benlliure J., Bernas M., Boudard A., Czajkowski S., et al. Light nuclides produced in the proton-induced spallation of U 238 at 1 GeV. Physical Review C. 73(1) (2006) p.014607.

55. Taieb J., Schmidt K.H., Tassan-Got L., Armbruster P., Benlliure J., Bernas M., et al. Evaporation residues produced in the spallation reaction 238U+ p at 1 A GeV. Nuclear Physics A. 724(3–4) (2003) pp.413–430.

56. Ahmad N., Jaafar M.S., Bakhash M. and Rahim M. An overview on measurements of natural radioactivity in Malaysia. Journal of radiation research and applied sciences. 8(1) (2015) pp.136–141.

57. World Health Organization, 2010. Childhood lead poisoning.

58. Tseluikin V., Dzhumieva A., Tikhonov D., Yakovlev A., Strilets A., Tribis A., et al., 2022. Pulsed electrodeposition and properties of nickel-based composite coatings modified with graphene oxide. Coatings, 12(5), p.656.

59. Jansen T., Blass D., Hartwig S. and Dilger K., 2018. Processing of advanced battery materials—laser cutting of pure Lithium metal foils. Batteries, 4(3), p.37.

60. Iwaki M., 2002. Estimation of the atomic density of amorphous carbon using ion implantation, SIMS and RBS. Surface and Coatings Technology, 158, pp.377–381.

61. Báez–Pimiento S., Hernández–Rojas M.E. and Palomar–Pardavé M.E., 2015. Processing and characterization of open–cell aluminum foams obtained through infiltration processes. Procedia Materials Science, 9, pp.54–61.

62. Riyanto, D. and Widodo, S., 2020, September. Soil physical and chemical fertility dynamic under organic, semi organic and conventional rice farming systems on Termas Village, Sambung Macan District, Sragen Regency. In IOP Conference Series: Earth and Environmental Science (Vol. 518, No. 1, p. 012071). IOP Publishing.